



Enhancing efficiency for additive-free blade-coated small-molecule solar cells by thermal annealing

Pei-Ting Tsai ^a, Hsin-Fei Meng ^{a,*}, Yongsheng Chen ^{b,**}, Bin Kan ^b, Sheng-Fu Horng ^c

^a Institute of Physics, National Chiao Tung University, 1001 University Road, Hsinchu 300, Taiwan

^b Key Laboratory for Functional Polymer Materials and Centre for Nanoscale Science and Technology, Institute of Polymer Chemistry, College of Chemistry, Nankai University, Tianjin 300071, China

^c Institute of Electronic Engineering, National Tsing Hua University, 101, Section 2, Kuang-Fu Road, Hsinchu 300, Taiwan



ARTICLE INFO

Article history:

Received 9 January 2016

Received in revised form

18 May 2016

Accepted 25 June 2016

Available online 18 July 2016

Keywords:

Additive-free

Small-molecule

Thermal annealing

Organic solar cells

Blade coating

ABSTRACT

Blade coating was successfully applied to realise high-efficiency small-molecule organic solar cells (OSCs) with a solution-processed active layer comprising a small organic molecule DR3TBDTT with a benzo[1,2–b:4,5–b']dithiophene (BDT) unit as the central building block as the donor and [6,6]–phenyl–C₇₁–butyric acid methyl ester (PC₇₁BM) as the acceptor. Using chloroform as the solvent, a DR3TBDTT/PC₇₁BM blend active layer without an additive was effectively formed through blade coating. The power conversion efficiency (PCE) of small organic molecule solar cells was enhanced by 3.7 times through thermal annealing at 100 °C. This method produces OSCs with a high PCE of up to 6.69%, with an open circuit voltage (V_{oc}) of 0.97 V, a short-circuit current density (J_{sc}) of 12.60 mA/cm², and a fill factor (FF) of 0.55.

© 2016 Elsevier B.V. All rights reserved.

1. Introduction

Bulk heterojunction organic solar cells (OSCs) have attracted attention as a clean and renewable energy resource because of features such as low production cost, solution processability at high throughput, light weight, and flexibility [1–3]. Moreover, OSCs utilising small-molecule solar cells as donors and acceptors have gained considerable attention because of advantages over their polymer counterparts such as a well-defined molecular structure, a definite molecular weight, and high purity without batch to batch variations [4]. The highest power conversion efficiency (PCE) of OSCs based on small molecular donor/fullerene acceptors is greater than 7%–9% [4–12].

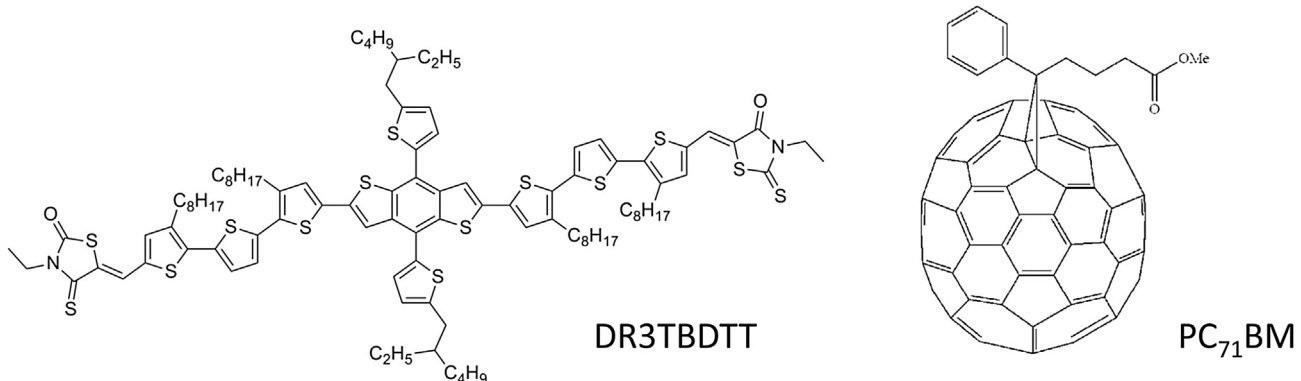
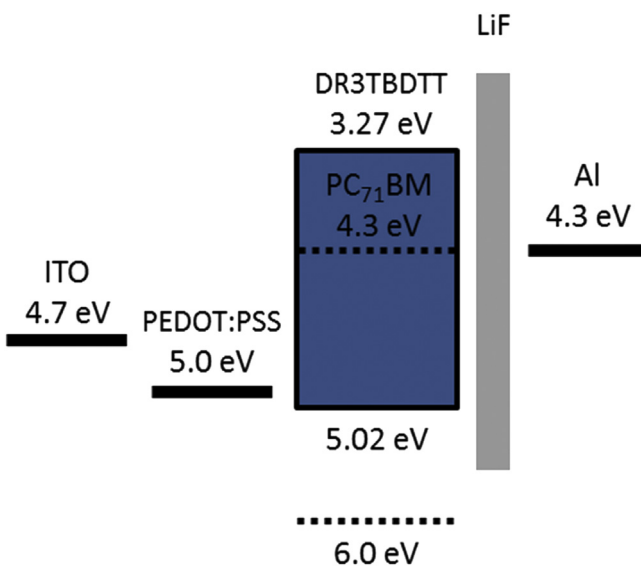
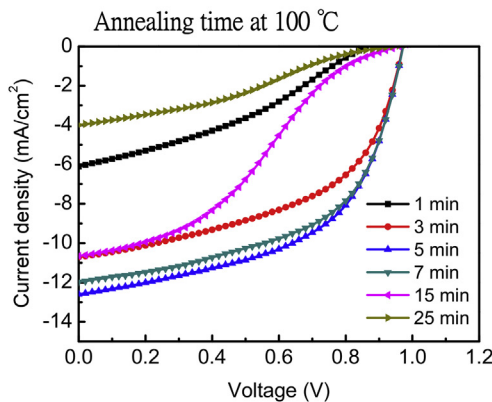
Amongst various methods for the optimisation of processing techniques, the most commonly used methods include thermal annealing [13–21] and the use of solvent additives [4–12,28–30]. Heat treatment causes the movement of molecules, resulting in the redistribution and eradication of the dislocations in bulk

heterojunctions. The enhanced device performance obtained under optimized annealing conditions is thought to be due partly to the improved light harvest and the interfacial contact between the metal electrode and the active layer and mainly to better donor/acceptor morphology in the active layer [22–25]. Many studies have been conducted to enhance efficiency through thermal annealing of P3HT and low-bandgap-material cells. However, the performance has not been enhanced appreciably. Most low band gap systems the efficiency becomes worse with annealing, but the opposite of P3HT. It may be that side chains have noteworthy influence on a polymer's properties, mainly its crystallinity and stability. In general, donor groups with side chain are the most susceptible to degradation while the most stable are those without side chains [26,27]. However, P3HT is a simple polymer which has high thermal stability. Therefore, low band gap systems the efficiency becomes worse with annealing and the opposite of what happens to P3HT may be attributed to their molecular structure. Moreover, high-efficiency OSCs are usually obtained using low percentages of solvent additives during the active layer film-forming process [4–12,28–30]. The additives cause nanoscale phase separation and a bicontinuous interpenetrating network in the active layer, which are critical for achieving appropriate phase-separated domains with highly efficient exciton dissociation and

* Corresponding author.

** Corresponding author.

E-mail addresses: meng@mail.nctu.edu.tw (H.-F. Meng), yschen99@nankai.edu.cn (Y. Chen).

**Fig. 1.** The chemical structures.**Fig. 2.** Energy band diagram.

carrier transport [30]. Nevertheless, the drying process of the residual high boiling point additives induces undesirable morphological variation as well as unfavourable interfacial contact [31]. In this study, the PCE of OSCs based on DR3TBDTT without additives was up to 6.69% after thermal annealing.

Practical application of organic photovoltaics relies on high-throughput processing. However, almost all device demonstration and fundamental research to date has utilised spin coating for thin film deposition. Spin-coated processing wastes a considerable amount of solution and is incompatible with large-scale processing and roll-to-roll fabrication. Blade coating has the advantages of large-area uniformity, a low amount of material waste, prevention of interlayer dissolution, and compatibility with the roll-to-roll process. Blade coating involves a rapid drying process that prevents the fabrication throughput from being slowed by conventional solvent annealing [32–42]. This study focused on the small-molecule donor DR3TBDTT [6]. Devices in which this donor was deposited through blade coating exhibited a high efficiency of 6.69% without additives after thermal annealing at 100 °C for 5 min, with an open circuit voltage (V_{oc}) of 0.97 V, a short-circuit current density (J_{sc}) of 12.60 mA/cm², and a fill factor (FF) of 0.55. The PCE of

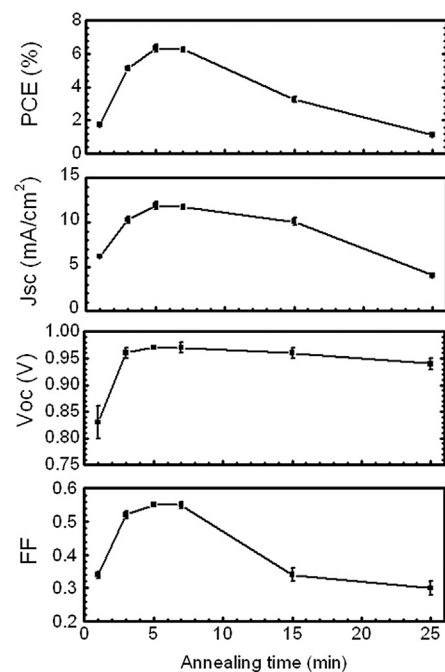
**Fig. 3.** J-V curves of DR3TBDTT/PC₇₁BM solar cells after thermal annealing at 100 °C for different time under illumination of AM 1.5 G, 100 mW/cm².

Table 1

The average device photovoltaic parameters for BHJ solar cells based on DR3TBDTT:PC₇₁BM after thermal annealing at 100 °C for different time.

Annealing time (min)	PCE (%)	J _{sc} (mA/cm ²)	V _{oc} (V)	FF
1	1.8	6.1	0.87	0.35
	1.7 ± 0.1	6.2 ± 0.1	0.83 ± 0.03	0.34 ± 0.01
3	5.4	10.7	0.97	0.52
	5.1 ± 0.2	10.3 ± 0.4	0.96 ± 0.01	0.52 ± 0.01
5	6.7	12.6	0.97	0.55
	6.4 ± 0.2	11.9 ± 0.5	0.97 ± 0.00	0.55 ± 0.00
7	6.4	12.0	0.97	0.55
	6.3 ± 0.1	11.7 ± 0.3	0.97 ± 0.01	0.55 ± 0.01
15	3.4	10.7	0.96	0.34
	3.3 ± 0.2	10.1 ± 0.4	0.96 ± 0.01	0.34 ± 0.02
25	1.2	4.0	0.94	0.32
	1.1 ± 0.0	4.0 ± 0.1	0.94 ± 0.01	0.3 ± 0.02

(polydimethylsiloxane) to the active–material chloroform solution. The active layer was blade coated at a constant speed of 140 mm/s and a solution of 50 μL was delivered to the blade gap of 120 μm, and the substrate temperature was 60 °C. The thermal annealing was carried out by placing the completed devices on a digitally controlled hotplate at different temperatures, in an nitrogen–filled glove box. Finally, a 0.8 nm LiF layer and 80 nm Al layer were successively deposited onto the active layer under high vacuum by a shadow mask to define the area of 0.04 cm² (<3 × 10⁻⁶ Pa). The deposition rate of LiF and Al were 0.1–Å/s and 2–Å/s, respectively. The sealant WB90US(P) was purchased from MORESCO Corporation. By using the sealants to seal the periphery of the devices between device and the sand-blast glass with hydroscopic. Subsequently, these devices were treated in an Ultra-

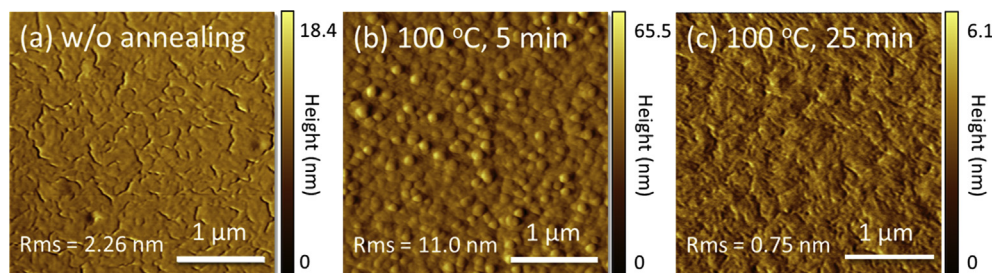


Fig. 4. AFM topography and phase images of DR3TBDTT/PC₇₁BM solar cells after thermal annealing at 100 °C for (a) 0 min, (b) 5 min, and (c) 25 min.

devices annealed at 100 °C for 5 min (6.69%) was 3.7 times higher than that of devices annealed for 1 min (1.82%). The devices are sensitive to the annealing temperature and time.

2. Experimental

2.1. Fabrication of DR3TBDTT–based organic solar cells

The OSCs based on small molecular donor and fullerene acceptors were fabricated on prepatterned ITO (indium–tin oxide) glass with device structures of ITO/PEDOT:PSS(40 nm)/DR3TBDTT:PC₇₁BM(100 nm)/LiF(0.8 nm)/Al(80 nm). The ITO–coated glass substrates were treated in an ultrasonic bath for 60 min in acetone, subsequently rinsed with deionized water for 5 min and cleaned using UV ozone cleaner for 20 min. PEDOT:PSS (poly–(3,4–ethylenedioxythiophene):poly–(styrenesulfonate) (CLEVIOS™ PVP AI4083, purchased from HC Starck, filtered at 0.22 μm) and IPA (isopropyl alcohol) were mixed at a volume ratio of 1:1. PEDOT:PSS layer was blade coated at a constant speed of 10 mm/s and a solution of 100 μL was delivered to the blade gap (30 μm) onto ITO substrate which was heated at 60 °C on a hotplate in air. After the PEDOT:PSS film was baked at 150 °C for 20 min, the substrates were transferred into an nitrogen–filled glove box. Subsequently, the active layer was blade–coated from blend chloroform solutions with weight ratio of DR3TBDTT with a benzo [1,2–b:4,5–b']dithiophene (BDT) unit as the central building block [6] and PC₇₁BM ([6,6]–phenyl–C₇₁–butyric acid methyl ester, purchased from Solenne) at 1:0.8. Fig. 1 shows the chemical structures of the active layer materials used. By extrapolation of the absorption onsets in the film state, the optical band gaps were estimated to be 1.72 for DR3TBDTT, which is consistent with the values of 1.75 eV, measured by cyclic voltammetry (CV). Fig. 2 shows DR3TBDTT has low band gap of 1.75 eV. The DR3TBDTT/PC₇₁BM+PDMS devices have the same weight ratio with the DR3TBDTT/PC₇₁BM device, and the addition of 0.2 mg/mL of PDMS

violet for 4 min. Finally, the devices with encapsulation can prevent water, which causes device degradation, from entering the devices.

2.2. Measurement and characterization of devices

To determine the characteristics of the solar cell devices, the power conversion efficiency (PCE) was measured using a solar simulator (XES–301S, SAN–EI) under AM 1.5G of irradiation. Average photovoltaic properties and their standard deviations for 4–8 cells from the same large area blend film, and equivalent circuit model parameters for the best cells prepared with different annealing temperatures and time. All cells have an active area of 0.04 cm². The incident photon conversion efficiency (IPCE) is

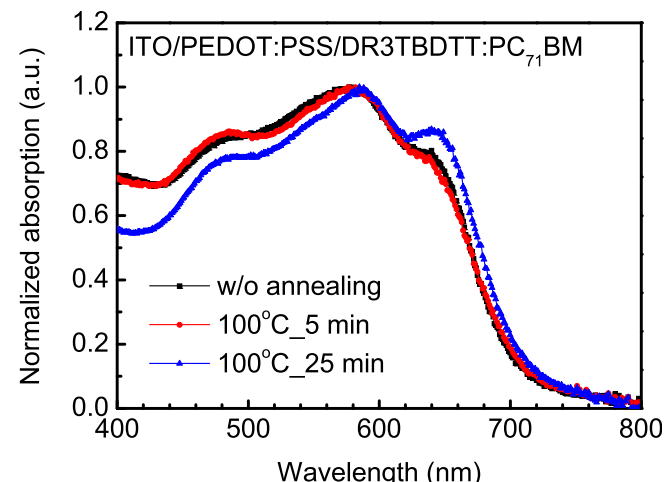


Fig. 5. The absorption spectra of films prepared with annealing time.

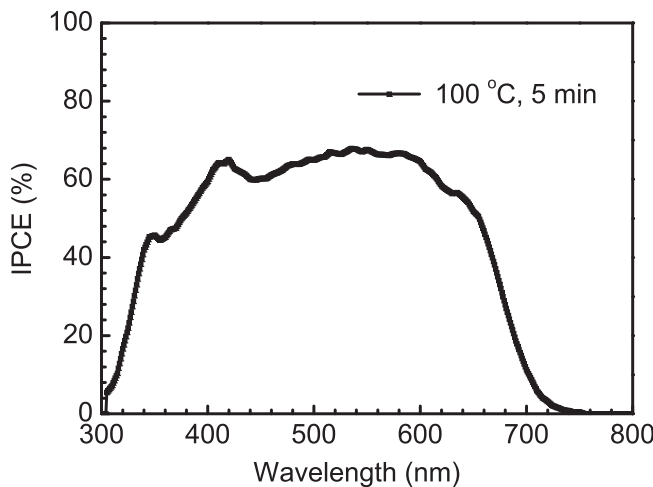


Fig. 6. IPCE spectrum of DR3TBDTT/PC₇₁BM solar cells after thermal annealing at 100 °C for 5 min.

defined as the average number of carriers per incident photon. To measure the IPCE, a 300-W Xenon lamp (Newport 66984) and a monochromator (Newport 74112) were used as light sources. The beam spot on the sample was a square, and the spot size was 3 mm². Calibration was conducted using a calibrated silicon photodetector with a known spectral response (Newport 818–UV). The IPCE was measured using a lock-in amplifier (Standard Research System, SR830), an optical chopper unit (SR540) operating at a 260-Hz chopping frequency, and a 1 Ω resistor in a shunt connection to convert the photocurrent to voltage. To analyze the films fabricated using various conditions, the surface morphology and phase images were monitored using an atomic force microscope (AFM, Dimension 3100, Digital Instruments). The high resolution morphology was monitored using a variable temperature scanning probe microscope (VT SPM, SPA–300HV). The absorption spectrum was measured using a UV–visible spectrophotometer

(HP8453). The devices of lifetime experiment were exposed in air at 60 °C with encapsulation under continuous illumination. The devices were connected to a power supply and a resistance and up to 1588 h continuous operation with fixed voltage of 0.8 V applied. Output current was approximately 0.25 mA (half of photo-current).

3. Results and discussion

3.1. Thermal annealing

Fig. 3 shows the current density–voltage (J–V) curves and trend of photovoltaic parameters of devices without additives after thermal annealing at 100 °C for different periods (under illumination of AM 1.5 G, 100 mW/cm²). The average device photovoltaic parameters for bulk heterojunction solar cells based on DR3TBDTT:PC₇₁BM after thermal annealing at 100 °C for different periods are summarised in Table 1. The highest PCE of the device with DR3TBDTT was 6.69%, with a J_{sc} of 12.60 mA/cm², a V_{oc} of 0.97 V and a FF of 0.55. The results indicated that the device performance was sensitive to the treatment time. All the devices except the devices annealed for 1 min exhibited a high V_{oc} (0.94–0.97 V). As the annealing time increased, the J_{sc} increased from 6.10 mA/cm² (1 min) to 12.60 mA/cm² (5 min) and then decreased to 4.00 mA/cm² (25 min). Similarly, the FF increased from 0.35 (1 min) to 0.55 (5 min) and then decreased to 0.32 (25 min). To characterise the morphology of the films that were blade coated for different annealing periods, atomic force microscopy was used to obtain topography images of the DR3TBDTT/PC₇₁BM films. The results after thermal annealing at 100 °C for different periods are shown in Fig. 4. The root mean square roughness values were 2.26, 11.0, and 0.75 nm for the films annealed at 100 °C for 0, 5, and 25 min, respectively. We surmise that roughness occurs on surface of active layer, involving grain boundaries and domains of phase separation. The film annealed for 5 min exhibited the highest roughness and largest grain size. The grains had a size of 100–150 nm and were visible only in the film annealed for 5 min. This large grain structure is most likely

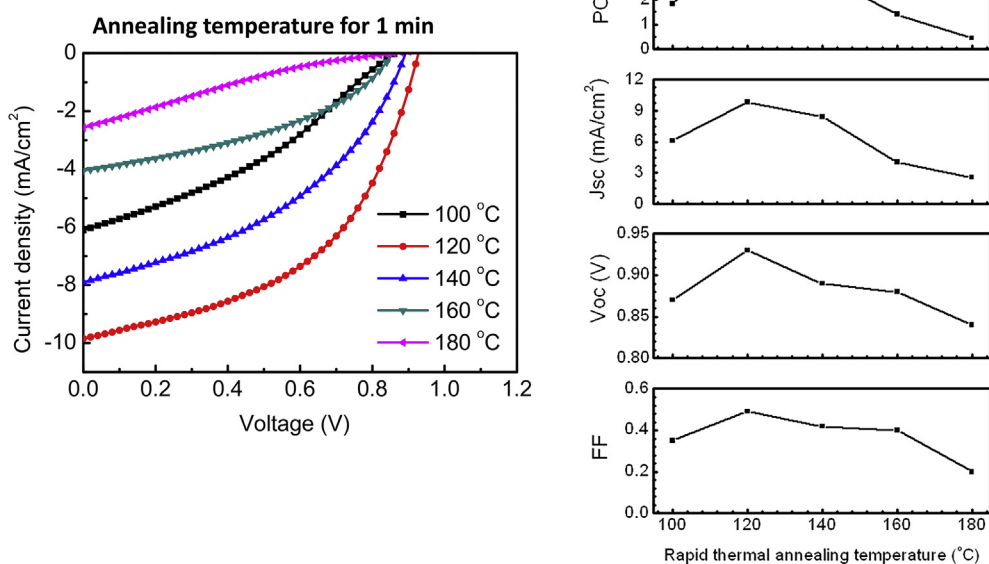


Fig. 7. J–V curves of DR3TBDTT/PC₇₁BM solar cells after rapid thermal annealing at various temperature.

Table 2

The average device photovoltaic parameters of DR3TBDTT/PC₇₁BM solar cells after rapid thermal annealing at various temperature.

Temperature (°C)	PCE (%)	J _{sc} (mA/cm ²)	V _{oc} (V)	FF
100 °C	1.8	6.1	0.87	0.35
	1.7 ± 0.1	6.2 ± 0.1	0.83 ± 0.03	0.34 ± 0.01
120 °C	4.5	9.8	0.93	0.49
	3.9 ± 0.4	9.31 ± 0.5	0.93 ± 0.01	0.45 ± 0.03
140 °C	3.0	8.5	0.89	0.42
	2.9 ± 0.1	8.18 ± 0.3	0.87 ± 0.02	0.41 ± 0.01
160 °C	1.4	4.1	0.88	0.40
	1.4 ± 0.0	4.00 ± 0.1	0.87 ± 0.01	0.40 ± 0.00
180 °C	0.5	2.6	0.84	0.20
	0.4 ± 0.0	2.55 ± 0.0	0.85 ± 0.02	0.20 ± 0.00

Table 3

The photovoltaic parameters of the DR3TBDTT/PC₇₁BM+PDMS devices after annealing at various temperature.

Annealing temperature (°C)	PCE (%)	J _{sc} (mA/cm ²)	V _{oc} (V)	FF
w/o annealing	3.0	7.8	1.00	0.38
60 °C	0.6	1.9	1.00	0.32
80 °C	0.2	1.3	0.99	0.13
100 °C	3.9	9.4	0.97	0.43
120 °C	3.7	8.0	0.96	0.48
140 °C	2.1	6.5	0.93	0.35

responsible for the high J_{sc} of the device annealed for 5 min, as shown in Fig. 4b. Upon an increasing in the annealing time from 0 to 5 min, a grain gradually formed; from 5 to 25 min, the grain boundary intensity gradually decreased. The blend films annealed for 5 min contain nanograins and have large surface areas, making

them efficient active layers that effectively contact the cathode and promote electron extraction and collection in devices. The bright domains may be DR3TBDTT rich and the dark domains were PC₇₁BM rich. The 30–40-nm DR3TBDTT domain size was well defined and had a strong connection. To obtain a clearer understanding of this strong dependence on annealing time, the absorption spectra of the device films without a cathode after thermal annealing at 100 °C for different periods were observed, and the results are shown in Fig. 5. The sample annealed for 25 min produced a pronounced long-wavelength shoulder peak at 638 nm, whereas the other two films did not produce a clear peak. This shoulder peak is generally attributed to the molecular aggregates in which the ordered chain packing produces a low amount of exciton energy. Annealing for a long time may cause the DR3TBDTT domain to have a high order or large size compared with short annealing. High-efficiency OSCs have an optimal range of phase separation; however, the devices annealed for 25 min had excessive ordering and phase separation leading to defects. This result may reflect that the chain stacking of polymers in the BHJ layers is dependent on the annealing time. The chain stacking of the DR3TBDTT component in the BHJ layer was relatively more prevented by the presence of the PC₇₁BM component when the annealing time was long. 25-min devices may have too much ordering and phase separation leading to the charge recombination and thus eliminates photocurrent. Therefore, thermal annealing can be a simple and effective method for improving the PCE of OSCs and has clear advantages for large-scale production. Fig. 6 shows the incident photon-to-electron conversion efficiency (IPCE) spectrum of DR3TBDTT/PC₇₁BM solar cells after thermal annealing at 100 °C for 5 min. The use of a higher chopping frequency and the light intensity of the solar simulator may have caused an error, and thus, a difference in photocurrent values was observed. The J_{sc} of the most efficient devices calculated

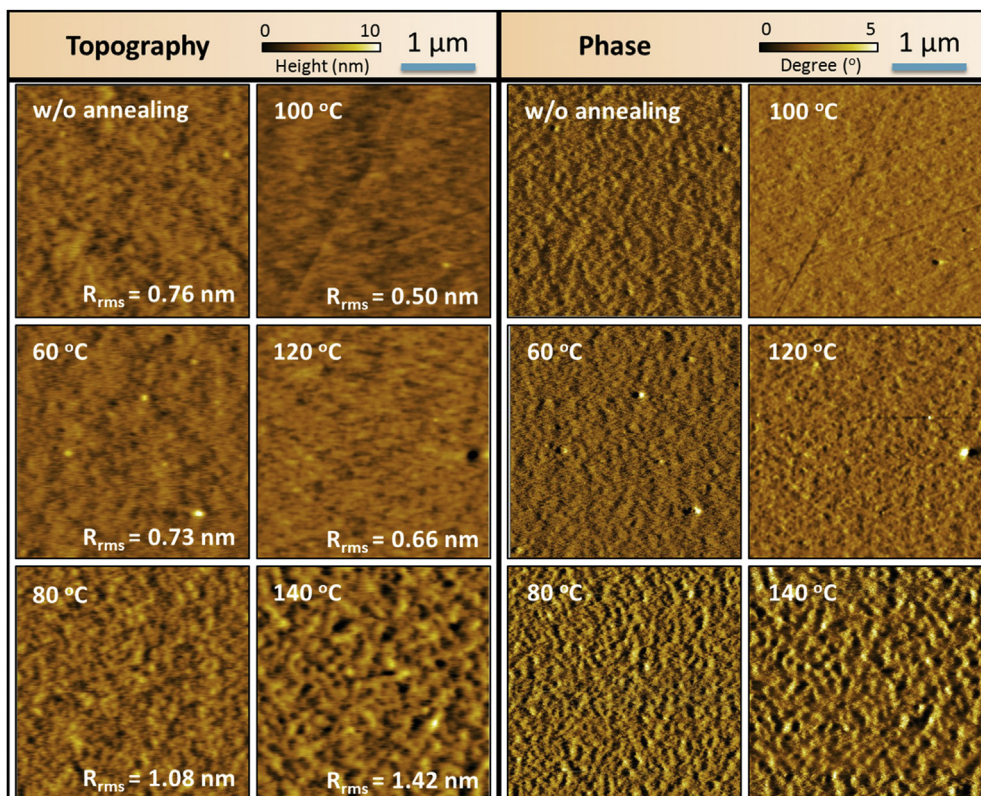


Fig. 8. AFM topography and phase images of DR3TBDTT/PC₇₁BM + PDMS solar cells after thermal annealing at various temperature.

by integrating the IPCE spectrum was 13.8 mA/cm^2 , whereas that measured using the J–V curve was 12.6 mA/cm^2 . The tolerance for the photocurrent measurement was approximately 8%.

3.2. Rapid thermal annealing

An alternative way to control the morphology of the DR3TBDTT/PC₇₁BM films is a rapid thermal annealing at various temperature for 1 min. Fig. 7 shows J–V curves of DR3TBDTT/PC₇₁BM solar cells after rapid thermal annealing at various temperatures; the photovoltaic parameters are summarised in Table 2. As the annealing temperature increased, the J_{sc} increased from 6.10 mA/cm^2 (100°C) to 9.84 mA/cm^2 (120°C) and then decreased to 2.57 mA/cm^2 (180°C). The FF increased from 0.35 (100°C) to 0.49 (120°C) and then decreased to 0.20 (180°C). Similarly, the V_{oc} increased from 0.87 (100°C) to 0.93 (120°C) and then decreased to 0.84 (180°C). In this case, the device at 120°C had the highest PCE of 4.48%. The results implied that the devices are sensitive to the annealing temperature and time, and rapid thermal annealing at a higher temperature in a very short time to enhance device performance must be considered. However, rapid thermal annealing had a negative effect when the device was subjected to a temperature higher than 140°C . This rapid thermal annealing temperature was so high that defects formed. These defects in the regular arrangement of the atoms act as temporary traps for charge carriers and thus reduce the amount of the usable photocurrent that can be produced.

3.3. Additive (PDMS)

High-efficiency OSCs are generally obtained by using low percentages of solvent additives during the active layer film-forming process [4–12,28–30]. The additives cause nanoscale phase separation and a bicontinuous interpenetrating network in the active layer, which are critical for achieving appropriate phase-separated domains with highly efficient exciton dissociation and carrier transport [30]. Nevertheless, the slow drying process of the residual high boiling point additives induces undesirable morphological variation as well as unfavourable interfacial contact. The photovoltaic parameters of the DR3TBDTT/PC₇₁BM+PDMS devices fabricated using blade coating are summarised in Table 3. The highest PCE of the DR3TBDTT/PC₇₁BM+PDMS devices after thermal annealing at 100°C for 10 min was 3.89%, with a J_{sc} of 9.38 mA/cm^2 , a V_{oc} of 0.97 V, and an FF of 0.43. The topography and phase images of the DR3TBDTT/PC₇₁BM+PDMS films at different thermal annealing temperatures are shown in Fig. 8. All the samples exhibited low root mean square roughness values and nanoscale phase separation. We surmise that the phase images do not show donor/acceptor phase separation but PDMS aggregation in Fig. 8. The residual PDMS may lead to violent aggregation at high temperature. It may be not good for the performance of device.

3.4. Lifetime

To evaluate the stability of the solar cells based on DR3TBDTT, the devices were exposed to air at 60°C with encapsulation under illumination. A photovoltaic parameter–operating time diagram is shown in Fig. 9. After 168 h of aging, the PCE of the DR3TBDTT/PC₇₁BM-based device decreased from 6.29% to 4.17%, with an approximately 25% reduction relative to the initial PCE. The V_{oc} , J_{sc} , and FF decreased from 0.97 to 0.96 V, 11.72 mA/cm^2 , and 0.55 to 0.41, with approximately 2%, 10%, and 25% reductions relative to the initial values, respectively. The J_{sc} and FF rapidly decreased with time at the beginning of the operating period. After 916 h of aging, the PCE decreased to 1.77%, with an approximately

75% reduction relative to the initial PCE, and was tending towards stability. The V_{oc} , J_{sc} , and FF decreased to 0.91 V, 8.34 mA/cm^2 , and 0.23, with approximately 6%, 29%, and 76% reductions relative to the initial values, respectively. These results suggested that the FF and J_{sc} were crucial for the degradation of PCE in this study. All the devices had well-defined encapsulation of hygroscopic layers, and therefore, chemical degradation through air exposure and water absorption by hygroscopic photoactive layers were negligible. Factors such as the photo-oxidation of active layers and metal electrodes under light illumination alter the overall photovoltaic performance and stability of organic material-based solar cell devices as a function of time under different ambient conditions [43]. Fig. 9 shows that FF and J_{sc} were key point for the degradation of PCE in this work. In general, donor groups with side chain are the most susceptible to degradation while the most stable are those without side chains [26,27]. DR3TBDTT has many side chains apparently. On the other hand, the degradation of interfaces was also a key issue. The stability test showed that the lifetime of the optimized device was very poor, which was attributed to the degradation of interfaces (ITO/PEDOT:PSS, PEDOT:PSS/organic, and organic/cathode). Donor and acceptor phase separation and morphology ... etc. affect the degradation. The lifetime of the devices based on DR3TBDTT in this study was excessively short for extensive use of organic photovoltaics. The interface between the

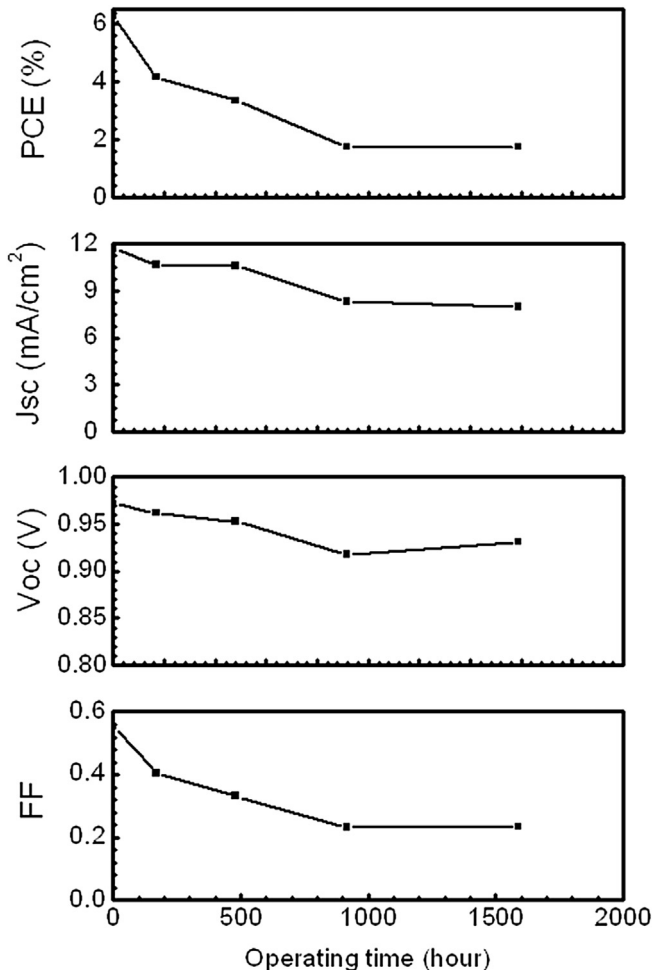


Fig. 9. Evolution of photovoltaic parameters of devices which were exposed in air for approximately 1600 h at 60°C with encapsulation under illumination. Devices were continuous operation with fixed voltage of 0.8 V applied. Output current was approximately 0.25 mA (half of photo-current).

active layer with a high scale roughness and the cathode with 0.8-nm LiF/100-nm Al may lead to contact degradation. A multilayer structure, such as a structure containing an electron transport layer, may enhance the lifetime of OSCs based on DR3TBDTT.

4. Conclusions

We demonstrated that the overall device performance of organic small-molecule solar cells can be considerably enhanced through thermal annealing. Rapid thermal annealing in a short time is effective in controlling the morphology and performance. Blade coating was successfully applied to realise high-efficiency small-molecule OSCs with a solution-processed active layer without additives. Additive-free solar cells have no residual additives, which lead to undesirable morphological variation, unfavourable interfacial contact, and process instability. The proposed method produces OSCs with high PCEs of up to 6.69%. The PCEs of these devices fabricated through blade coating are comparable with those of the reported DR3TBDTT/PC₇₁BM OSCs prepared using spin coating and additives.

Acknowledgement

This work was supported by Ministry of Science and Technology of Taiwan under Grant Nos. 104–2119–M–009–012 – and 104–2112–M–009–009–MY3. We thank Peichen Yu for the IPCE system.

References

- [1] Y.W. Su, S.C. Lan, K.H. Wei, Mater Today 15 (2012) 554–562.
- [2] G. Li, R. Zhu, Y. Yang, Nat. Photonics 6 (2012) 153–161.
- [3] P. Kumar, S. Chand, Prog. Photovoltaics 20 (2012) 377–415.
- [4] Y. Lin, Y. Li, X. Zhan, Chem. Soc. Rev. 41 (2012) 4245–4272.
- [5] Z. Du, W. Chen, Y. Chen, S. Qiao, X. Bao, S. Wen, M. Sun, L. Han, R. Yang, J. Mater. Chem. A 2 (2014) 15904–15911.
- [6] J. Zhou, Y. Zuo, X. Wan, G. Long, Q. Zhang, W. Ni, Y. Liu, Z. Li, G. He, C. Li, B. Kan, M. Li, Y. Chen, J. Am. Chem. Soc. 135 (2013) 8484–8487.
- [7] Y. Liu, C. Chen, Z. Hong, J. Gao, Y.M. Yang, H. Zhou, L. Dou, G. Li, Y. Yang, Sci. Rep. 3 (2013) 3356.
- [8] A.K.K. Kyaw, D.H. Wang, V. Gupta, J. Zhang, S. Chand, G.C. Bazan, A.J. Heeger, J. Adv. Mater. 25 (2013) 2397–2402.
- [9] J. Zhou, X. Wan, Y. Liu, Y. Zuo, Z. Li, G. He, G. Long, W. Ni, C. Li, X. Su, Y. Chen, J. Am. Chem. Soc. 134 (2012) 16345–16351.
- [10] A.K.K. Kyaw, D.H. Wang, V. Gupta, W.L. Leong, L. Ke, G.C. Bazan, A.J. Heeger, ACS Nano 7 (2013) 4569–4577.
- [11] L. Li, L. Xiao, H. Qin, K. Gao, J. Peng, Y. Cao, F. Liu, T.P. Russell, X. Peng, ACS Appl. Mater. Interfaces 7 (2015) 21495–21502.
- [12] X. Ouyang, R. Peng, L. Ai, X. Zhang, Z. Ge, Nat. Phot. 9 (2015) 520–525.
- [13] G. Li, V. Shrotriya, J. Huang, Y. Yao, T. Moriarty, K. Emery, Y. Yang, Nat. Mater. 4 (2005) 864–868.
- [14] L. Zheng, J. Liu, Y. Ding, Y. Han, J. Phys. Chem. B 115 (2011) 8071–8077.
- [15] Z. Huang, E.C. Fregoso, S. Dimitrov, J.R. Durrant, J. Mater. Chem. A 2 (2014) 19282–19289.
- [16] B. Walker, A.B. Tamayo, X.D. Dang, T.Q. Nguyen, Adv. Funct. Mater. 1 (2009) 3063–3069.
- [17] B.A. Rao, K. Yesudas, G.S. Kumar, K. Bhanuprakash, V.J. Rao, G.D. Sharma, S.P. Singh, Photochem. Photobiol. Sci. 12 (2013) 1688–1699.
- [18] N. Herath, S. Das, J.K. Keum, J. Zhu, R. Kumar, I.N. Ivanov, B.G. Sumpter, J.F. Browning, K. Xiao, G. Gu, P. Joshi, S. Smith, V. Lauter, Sci. Rep. 5 (2015) 13407.
- [19] C.V. Kumer, L. Cabau, E.N. Koukaras, G.D. Sharma, E. Palomares, Org. Electron. 26 (2015) 36–47.
- [20] H. Chen, J. Miao, J. Yan, Z. He, H. Wu, IEEE J. Sel. Top. quantum Electron. 22 (1) (2016).
- [21] M.S. Ryu, H. Jin Cha, J. Jang, Curr. Appl. Phys. 10 (2010) S206–S209.
- [22] H. Kim, W. So, S. Moon, J. Korean Phys. Soc. 48 (3) (2006) 441–445.
- [23] Y.-C. Huang, S.-Y. Chuang, M.-C. Wu, H.-L. Chen, C.-W. Chen, W.-F. Su, J. Appl. Phys. 106 (2009) 034506.
- [24] E. Verploegeen, R. Mondal, C.J. Bettinger, S. Sok, M.F. Toney, Z. Bao, Adv. Funct. Mater. 20 (2010) 3519–3529.
- [25] A.J. Pearson, T. Wang, R.A.L. Jones, D.G. Lidzey, Macromolecules 45 (2012) 1499–1508.
- [26] M. Manceau, E. Bundgaard, J.E. Carlé, O. Hagemann, M. Helgesen, R. Søndergaard, M. Jørgensen, F.C. Krebs, J. Mater. Chem. 21 (2011) 4132–4141.
- [27] R. Roesch, T. Faber, E. von Hauff, T.M. Brown, M. Lira-Cantu, H. Hoppe, Adv. Energy Mater. (2015) 1501407.
- [28] W. Huang, E. Gann, L. Thomsen, C. Dong, Y.-B. Cheng, C.R. McNeill, Adv. Energy Mater. 5 (2015).
- [29] L. Huo, S. Zhang, X. Guo, F. Xu, Y. Li, J. Hou, Angew. Chem. Int. Ed. 50 (2011) 9697–9702.
- [30] H.-C. Liao, C.-C. Ho, C.-Y. Chang, M.-H. Jao, S.B. Darling, W.-F. Su, Mater. Today 16 (2013) 326–336.
- [31] L. Ye, Y. Jing, X. Guo, H. Sun, S. Zhang, M. Zhang, L. Huo, J. Hou, J. Phys. Chem. C 117 (2013) 14920–14928.
- [32] Y.-H. Chang, S.-R. Tseng, C.-Y. Chen, H.-F. Meng, E.-C. Chen, S.-F. Horng, C.-S. Hsu, Org. Electron. 10 (2009) 741–746.
- [33] C.-Y. Chen, H.-W. Chang, Y.-F. Chang, B.-J. Chang, Y.-S. Lin, P.-S. Jian, H.-C. Yeh, H.-T. Chien, E.-C. Chen, Y.-C. Chao, H.-F. Meng, H.-W. Zan, H.-W. Lin, S.-F. Horng, Y.-J. Cheng, F.-W. Yen, I.-F. Lin, H.-Y. Yang, K.-J. Huang, M.-R. Tseng, J. Appl. Phys. 110 (2011) 094501.
- [34] J.-H. Chang, Y.-H. Chen, H.-W. Lin, Y.-T. Lin, H.-F. Meng, E.-C. Chen, Org. Electron. 13 (2012) 705–709.
- [35] J.-H. Chang, Y.-H. Chen, H.-W. Lin, Y.-T. Lin, H.-F. Meng, E.-C. Chen, Sol. Energy Mater. Sol. Cells 107 (2012) 292–297.
- [36] Y.-F. Chang, Y.-C. Chiu, H.-C. Yeh, H.-W. Chang, C.-Y. Chen, H.-F. Meng, H.-W. Lin, H.-L. Huang, T.-C. Chao, M.-R. Tseng, H.-W. Zan, S.-F. Horng, Org. Electron. 13 (2012) 2149–2155.
- [37] Y.-F. Chang, Y.-C. Chiu, H.-W. Chang, Y.-S. Wang, Y.-L. Shih, C.-H. Wu, Y.-L. Liu, Y.-S. Lin, H.-F. Meng, Y. Chi, H.-L. Huang, M.-R. Tseng, H.-W. Lin, H.-W. Zan, S.-F. Horng, Y.-J. Juang, J. Appl. Phys. 114 (2013) 123101.
- [38] Y.-R. Hong, P.-K. Chen, J.-C. Wang, M.-K. Lee, S.-F. Horng, H.-F. Meng, Sol. Energy Mater. Sol. Cells 120 (2014) 197–203.
- [39] H.-W. Lin, J.-H. Chang, W.-C. Huang, Y.-T. Lin, L.-Y. Lin, F. Lin, K. -Tsung Wong, H.-F. Wang, R.-M. Ho, H.-F. Meng, J. Mater. Chem. A 2 (2014) 3709–3714.
- [40] P.-T. Tsai, C.-Y. Tsai, C.-M. Wang, Y.-F. Chang, H.-F. Meng, Z.-K. Chen, H.-W. Lin, H.-W. Zan, S.-F. Horng, Y.-C. Lai, P. Yu, Org. Electron. 15 (2014) 893–903.
- [41] P.-T. Tsai, K.-C. Yu, C.-J. Chang, S.-F. Horng, H.-F. Meng, Org. Electron. 22 (2015) 166–172.
- [42] M. Li, F. Liu, X. Wan, W. Ni, B. Kan, H. Feng, Q. Zhang, X. Yang, Y. Wang, Y. Zhang, Y. Shen, T.P. Russell, Y. Chen, Adv. Mater. 27 (2015) 6296–6302.
- [43] E. Singh, H.S. Nalwa, RSC Adv. 5 (2015) 73575–73600.